

Multiple perfectly-transmitting states of a single-level at strong coupling

ÉTIENNE JUSSIAU^{(a)1,2} and ROBERT S. WHITNEY^{(b)2}

¹ Department of Physics and Astronomy, University of Rochester, Rochester, NY 14627, USA

² Laboratoire de Physique et Modélisation des Milieux Condensés, Université Grenoble Alpes and CNRS, 25 Avenue des Martyrs, BP 166, 38042 Grenoble, France.

PACS 73.23.-b – Electronic transport in mesoscopic systems

PACS 84.40.Dc – Microwave circuits

Abstract – We study transport through a single-level system placed between two reservoirs with band-structure, taking strong level-reservoir coupling of the order of the energy-scales of these band-structures. An exact solution in the absence of interactions gives the nonlinear Lamb shift. As expected, this moves the perfectly-transmitting state (the reservoir state that flows through the single-level without reflection), and can even turn it into a bound-state. However, here we show that it can also create additional pairs of perfectly-transmitting states at other energies, when the coupling exceeds critical values. Then the single-level’s transmission function resembles that of a multi-level system. Even when the discrete level is outside the reservoirs’ bands, additional perfectly-transmitting states can appear inside the band when the coupling exceeds a critical value. We propose observing the bosonic version of this in microwave cavities, and the fermionic version in the conductance of a quantum dot coupled to 1D or 2D reservoirs.

Introduction. – There is currently great interest in strong coupling between small systems and reservoirs [1–9], for both practical and fundamental reasons. It is of practical interest in electron nanostructures; for example for lower resistance electronics (resistance being inversely proportional to coupling strength), and more powerful nanoscale thermoelectric heat engines and refrigerators [10]. It is of fundamental interest, because it leads to physics which one could not guess from either the small system’s properties or the reservoir’s properties. In such cases, the reservoir can induce long time correlations in the small system’s evolution, making it non-Markovian, and thus challenging to model.

In this work, we show that strong coupling has a striking effect on *perfectly-transmitting states*. These are reservoir states that exhibit perfect (reflectionless) flow from one reservoir to another through a small system. We consider the small system to be a single-level system (or single-mode cavity) as in Figs. 1 & 2. We show that the perfectly-transmitting states are intimately related to *bound-states*, despite having the opposite properties (bound states carry no steady-state flow between reser-

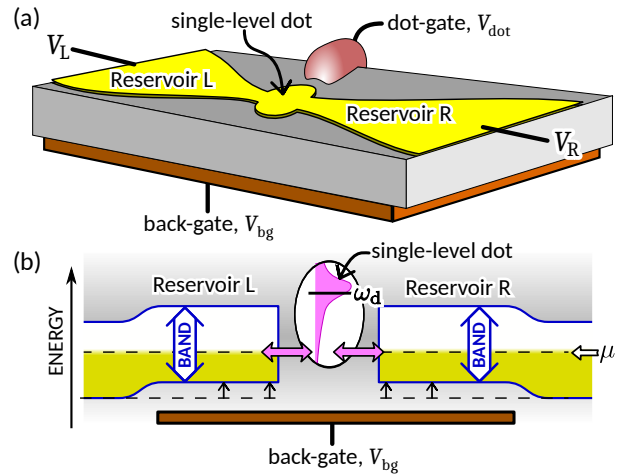


Fig. 1: (a) A single-level quantum dot between two 2-dimensional electronic reservoirs; the reservoirs could equally be 1D wires. (b) The back-gate is used to shift the reservoir’s band with respect to the electro-chemical potential, μ . The dot-gate controls the energy of the dot-level, ω_d . The purple Lorentzian is the golden-rule picture, which *cannot* explain the perfectly-transmitting states that we find.

^(a) ejussiau@UR.Rochester.edu

^(b) robert.whitney@grenoble.cnrs.fr

voirs¹). Such bound-states are a known (but intriguing) consequence of strong-coupling to a reservoir with a band-gap, giving non-Markovian dynamics to the single-level system [12]. Then a particle placed in the single-level system never fully decays into the continuum even when it has the energy to do so [13–19]. Bound-states were first predicted for an impurity in a superconductor [20], or an electronic tight-binding model [21]. They were studied for the Wigner-Weisskopf model of an atomic level coupled to a photonic vacuum with band-structure [13–16], reviewed in Refs. [17, 18], with generalizations to a finite-temperature Fano-Anderson model [12, 19, 22–24]. Their properties were explored in models of quantum dots coupled to electronic reservoirs [11, 12, 19, 25–32]. Recent experiments probed them in NV centres in a waveguide [33], and for matter waves in ultracold atoms [34]. While such bound-states have rich physics, we show that the physics of *perfectly-transmitting states* is similar, but richer.

Our main result is that additional perfectly-transmitting states appear via transitions that occur when the coupling exceeds critical values. Then a single-level’s transmission function resembles that of a multi-level system. The most striking example is when the level’s energy is outside the reservoirs’ band. Once the coupling exceeds a critical value, additional perfectly-transmitting states appear within the band, ensuring perfect (reflectionless) flow between the reservoirs, even though the flow is through a level at an energy outside the band.

Perfectly-transmitting states in golden-rule. –

At weak-coupling, the perfectly-transmitting state of a single-level system is described by Fermi’s golden rule [35]. For extremely weak coupling, resonant transmission happens at the energy of this level, so there is a perfectly-transmitting state at this energy. The golden rule then implies that as the coupling increases, this state is broadened and Lamb shifted. However, this argument does not predict more than one perfectly-transmitting state per discrete-level, unlike our exact calculation.

If the single-level has an energy outside the reservoir’s band, then this golden-rule argument would predict that the level is Lamb shifted away from the band (level-repulsion between the level and the reservoir modes), while it broadens into a Lorentzian. This would suggest that transmission between reservoirs only occurs through the Lorentzian’s tail (see Fig. 1b). Hence, this golden-rule argument cannot explain the perfectly-transmitting states that appear in our exact calculation, see Fig. 3.

This golden-rule argument fails due to its neglect of the energy dependence of the Lamb shift, induced by the reservoirs’ band-structure. It is the nonlinearity of this energy

¹We consider the dc (zero-frequency) component of the current, established at long times after turning on the coupling. This clarification is important because bound-states can induce finite-frequency oscillations which survive in the long-time limit, if the coupling is turned on non-adiabatically [9, 11].

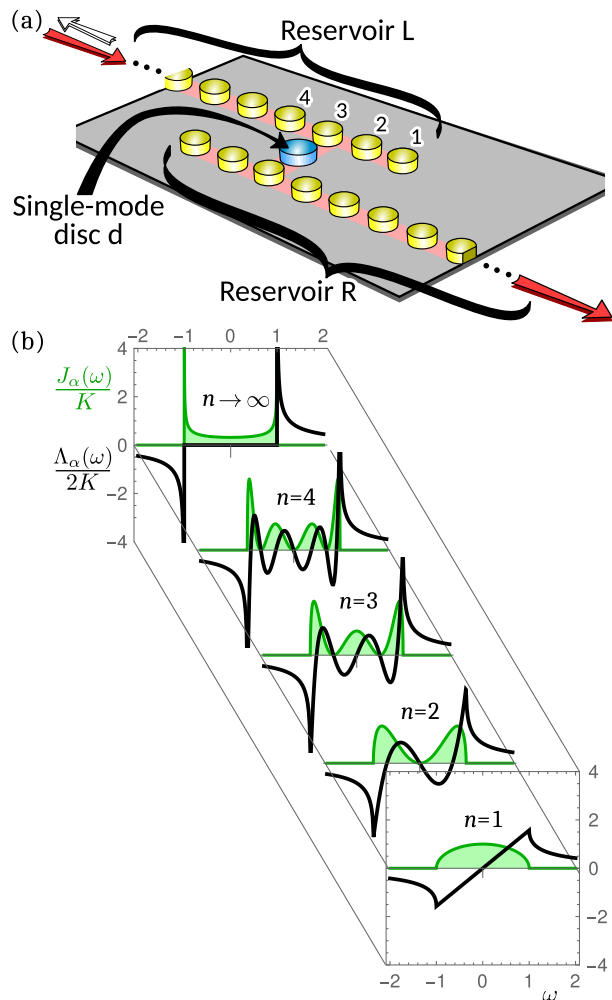


Fig. 2: (a) A microwave system in which the single-level is the single-mode of disc d, while each reservoir is a chain of single-mode dielectric discs (yellow), with weak coupling to the nearest neighbour in the chain (indicated by pink bands). Disc d’s single-mode is at an energy which differs by ω_d from those in the reservoir chains, and it couples to the n th disc in each reservoir (the sketch shows $n = 3$) with coupling strength K . (b) The spectral function and Lamb shift when disc d is coupled to the n th disc in the chain, plotted as $J_\alpha(\omega)/K$ in green and $\Lambda_\alpha(\omega)/(2K)$ in black (the factor of 2 is to make $J_\alpha(\omega)$ and $\Lambda_\alpha(\omega)$ appear clearly in the same plot).

dependence that gives rise to transitions at which new perfectly-transmitting states appear.

Hamiltonian and transmission function. – We consider the Fano-Anderson model [21, 36–38] for a single-level system coupled to two reservoirs; left (L) and right (R). This model applies to electrons (Fig. 1) in the absence of spin and interaction effects², or with interactions treated in the Hartree approximation [37]. It also applies to photons [36, 38] (Fig. 2a), or other non-interacting

²The model applies to quantum dots with on-site Coulomb interactions, so long as the magnetic field is strong enough that the spin-state with higher energy is always empty.

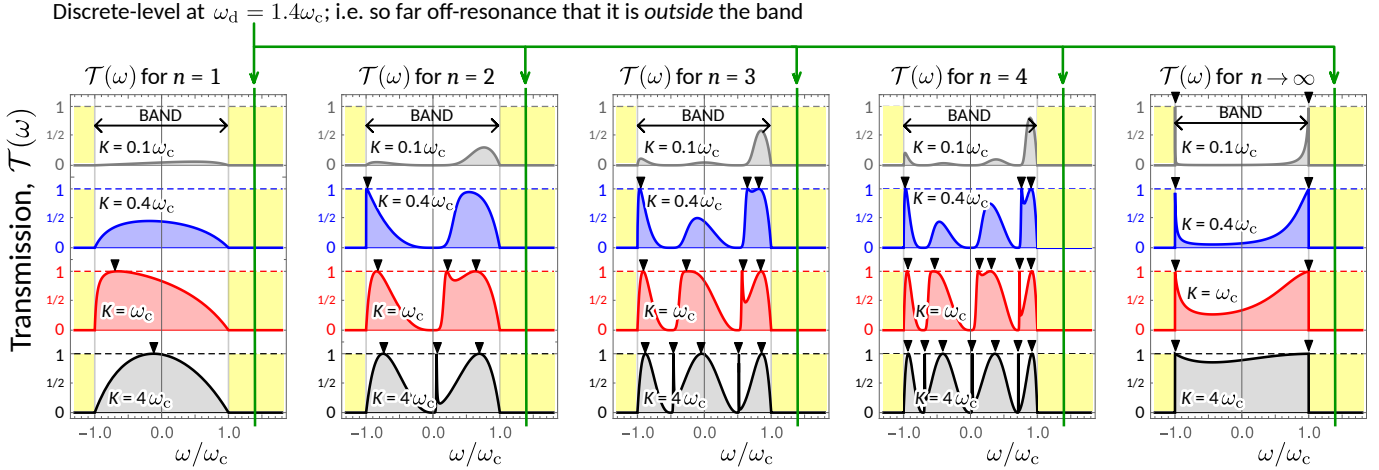


Fig. 3: Transmission functions when the single-level is outside the reservoir’s band at $\omega_d = 1.4\omega_c$. Despite this, there are perfectly-transmitting states inside the band (indicated by inverted black triangles), at strong enough coupling. The plots are for systems with the spectral functions, $J_L(\omega) = J_R(\omega)$ given by Eq. (8), as for the system in Fig. 2, with $n = 1, 2, 3, 4, \infty$. Note that the bound-states do not appear here because they do not contribute to the transmission; when they are present, they are outside the band (sitting in the yellow zones).

bosons [30]. The model’s Hamiltonian is

$$\hat{H} = \omega_d \hat{d}^\dagger \hat{d} + \sum_{\alpha,k} \left(\omega_{\alpha k} \hat{c}_{\alpha k}^\dagger \hat{c}_{\alpha k} + g_{\alpha k} \hat{d}^\dagger \hat{c}_{\alpha k} + g_{\alpha k}^* \hat{c}_{\alpha k}^\dagger \hat{d} \right), \quad (1)$$

where \hat{d}^\dagger and \hat{d} are creation and annihilation operators for the single-level system state, while $\hat{c}_{\alpha k}^\dagger$ and $\hat{c}_{\alpha k}$ are creation and annihilation operators for the k th mode of reservoir $\alpha \in \{L, R\}$. The discrete state has energy ω_d , and has a coupling $g_{\alpha k}$ to the k th mode in reservoir α , which has energy $\omega_{\alpha k}$. The creation and annihilation operators are fermionic for electrons, while they are bosonic for photons. In either case, each reservoir contains infinitely many modes described by continuous spectral functions,

$$J_\alpha(\omega) = \sum_k |g_{\alpha k}|^2 \delta(\omega - \omega_{\alpha k}). \quad (2)$$

Physically, this spectral function is equal to the reservoir’s local density-of-states on its surface where it exchanges particles with the discrete-level, multiplied by the tunnelling amplitude, $|g_{\alpha k}|^2$. For convenience, we define a dot-reservoir coupling K_α as the typical magnitude of $J_\alpha(\omega)$ (its exact definition will be given below for specific reservoir spectra). We do *not* take the wide-band limit, and instead consider the coupling K_α to be of the order of the band-width. This typically requires K_α to be of similar magnitude to the inter-site coupling inside the reservoir.

An exact solution to the model defined by Eqs. (1,2) using non-equilibrium Green’s functions [11, 28, 39, 40] or simply using Heisenberg equations of motion [2, 9], gives the dc particle and energy currents (see footnote ¹),

$$j_{\text{dc}}^{(\kappa)} = \int_{-\infty}^{\infty} \frac{d\omega}{h} \omega^\kappa \mathcal{T}(\omega) (f_L(\omega) - f_R(\omega)), \quad (3)$$

where $f_\alpha(\omega)$ is reservoir α ’s distribution function, with $\kappa = 0$ for particle current and $\kappa = 1$ for energy current. Hence, this exact calculation gives currents that take the form of a Landauer formula [39, 41–43]. The transmission function, $\mathcal{T}(\omega)$, is the probability that a particle at energy ω transmits from one reservoir to the other through the single-level. The exact solution gives [2, 9, 40, 44],

$$\mathcal{T}(\omega) = \frac{4\pi^2 J_L(\omega) J_R(\omega)}{(\omega - \omega_d - \Lambda(\omega))^2 + \pi^2 (J_L(\omega) + J_R(\omega))^2}, \quad (4)$$

for all ω where $J_{L,R}(\omega) \neq 0$, with $\mathcal{T}(\omega) = 0$ otherwise. Eq. (4) is a distorted Lorentzian if $J_\alpha(\omega)$ and $\Lambda(\omega)$ only depend weakly on ω , but we will show that it can take very different shapes for strong ω dependences. For any ω -dependence, it obeys $0 \leq \mathcal{T}(\omega) \leq 1$ for all ω . Here $\Lambda(\omega) = \Lambda_L(\omega) + \Lambda_R(\omega)$ is the Lamb shift, given by the principal value integral

$$\Lambda_\alpha(\omega) = \mathcal{P} \int d\omega' \frac{J_\alpha(\omega')}{\omega - \omega'}. \quad (5)$$

For photonic reservoirs, $\mathcal{T}(\tilde{\omega})$ is directly observable from Eq. (3) by injecting a monochromatic beam at frequency $\tilde{\omega}$ into the system; so $f_L(\omega) \propto \delta(\omega - \tilde{\omega})$ and $f_R(\omega) = 0$. For electronic reservoirs, one measures this transmission function by going to low temperature and small bias, where Eq. (3) gives the electrical current $I_{\text{dc}} = e j_{\text{dc}}^{(0)} = GV$ with conductance

$$G = e^2 \mathcal{T}(\mu) / h, \quad (6)$$

where μ is the reservoirs’ electrochemical potential. Then $\mathcal{T}(\omega)$ can be probed by measuring G while using a back-gate to move μ with respect to the reservoir bands [45–47] (see Fig. 1b). Note that to-date experiments that use the back-gate in this manner require that the reservoirs are one or two dimensional; nanowires, graphene, etc.

Perfectly-transmitting states and bound states.

– If the two reservoirs have the same spectral function, $J_L(\omega) = J_R(\omega)$, both the perfectly-transmitting states and the bound-states are given by the solutions of

$$\omega - \omega_d = \Lambda(\omega). \quad (7)$$

The solutions with ω s that fall in band-gaps (so $J_L(\omega) = J_R(\omega) = 0$) are well known to be bound-states [21, 38, 48]. Here we see all other solutions are perfectly-transmitting states, because they have $\mathcal{T}(\omega) = 1$ from Eq. (4) with $J_L(\omega) = J_R(\omega) \neq 0$. All such solutions can be found graphically by plotting $\Lambda(\omega)$, and seeing where it intersects the line $(\omega - \omega_d)$.

For any $J_\alpha(\omega)$, Eq. (5) shows that $\Lambda(\omega)$ decreases monotonically with ω in any band gap, so there is at most one bound state in any given band-gap [9]. In contrast, $\Lambda(\omega)$ can be non-monotonic inside bands, see Figs. 2b and 5a for examples. Then there can be multiple solutions of Eq. (7) inside a band, meaning multiple perfectly-transmitting states in that band. At strong coupling, their number equals the number of zeros of $\Lambda(\omega)$ inside that band. Often this is the maximum number of perfectly transmitting states, however there are models with more such states at weak or intermediate coupling (see Appendix C).

We concentrate on $J_L(\omega) = J_R(\omega)$ in this work. However, we note that there are no perfectly-transmitting states for $J_L(\omega) \neq J_R(\omega)$. Instead, solutions of Eq. (7) correspond to the maximum allowed transmission, $\mathcal{T}_{\max}(\omega) = 4J_L(\omega)J_R(\omega) / (J_L(\omega) + J_R(\omega))^2$; that is to say that no choice of ω_d that will give a larger $\mathcal{T}(\omega)$ at this ω .

Phase-diagrams. – By counting the solutions of the Eq. (7), we can construct “phase diagrams” of the number of perfectly-transmitting states and bound states as a function of the discrete level’s energy, ω_d , and the dot-reservoir coupling, K_α , as in Figs. 4 and 5c. Since $\Lambda(\omega)$ is a continuous function of ω , new solutions of Eq. (7) appear in pairs. At the same time all the solutions move with coupling. Hence, there are two main types of transitions. Transitions of type (i) are where a perfectly-transmitting state moves out of the continuum to become a bound state, as discussed in Ref. [9]. Transitions of type (ii) are those where an additional pair of perfectly-transmitting states is added. In this case, as the coupling approaches the phase boundary, a peak grows to form a perfectly-transmitting state at the phase boundary, which splits into two such states upon passing into the new phase.

There is also a non-generic transition, which we call type (iii), in which types (i) and (ii) occur together; i.e. a pair of states appear at the band edge, but one immediately moves out of the band to become a bound-state while the other moves into the band as a perfectly-transmitting state. It is non-generic because it only happens when $\Lambda(\omega)$ has a cusp at the band-edge, and its first and second derivative have the same sign on the band side of the cusp. However, this is the case for all the models in Fig. 2b, so type (iii) transitions occur there.

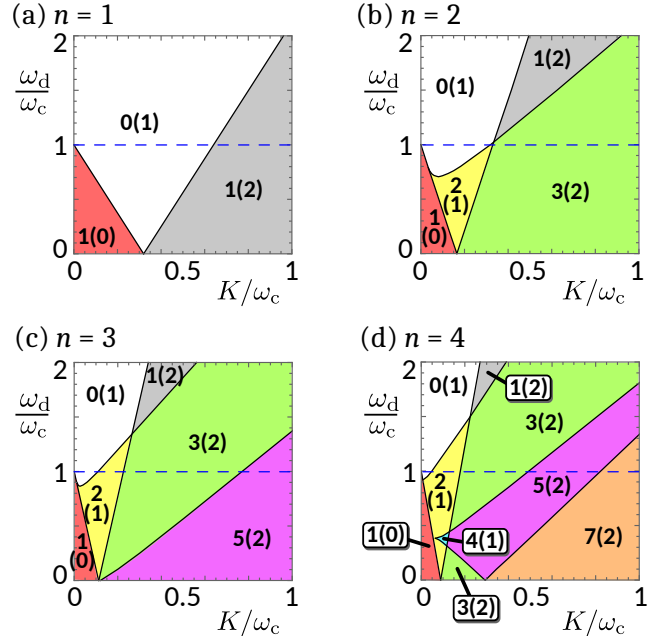


Fig. 4: Phase diagrams for the system in Fig. 2a when disc d is coupled to the n th disc in each 1D reservoir. Each “phase” labelled $k(l)$ where k is the number of perfectly-transmitting states and l is the number of bound-states.

Perfect transmission with level outside band. –

If ω_d is not within a band, then there are no perfectly-transmitting states at weak-coupling (assuming $J_\alpha(\omega)$ and $\Lambda(\omega)$ do not diverge). However, as the coupling is increased, transitions of type (ii) or (iii) can occur which generate one or more perfectly-transmitting states inside the band. Transitions from white to yellow in Fig. 4 are type (ii), while those from white to grey are type (iii).

In addition, for $J_L(\omega) = J_R(\omega)$ there are perfectly-transmitting states at any ω for which $J_L(\omega)$ diverges, if it diverges faster than $\Lambda(\omega)$. Then Eq. (4) gives $\mathcal{T}(\omega) = 1$ at this ω for all ω_d and all K_α , even $K_\alpha \rightarrow 0$ [9]; see e.g. $\mathcal{T}(\omega)$ at the band-edge for $n \rightarrow \infty$ in Fig. 3, due to $J_\alpha^{(n \rightarrow \infty)}(\omega)$ having a square-root divergence there.

Microwave tight-binding reservoirs. –

We imagine microwave experiments on tight-binding Hamiltonians like in Refs. [49–51], with high-refractive index dielectric discs arranged as in Fig. 2a, and sandwiched between two metallic plates. Each centimetre-sized disc supports a single GigaHertz mode, whose energy is tuned by changing the disc size. The discs couple to each other via evanescent waves in the air between the metallic plates, so the tunnel coupling can be tuned by changing the distance between discs. The two one-dimensional chains of identical discs play the role of the reservoirs, and they are both coupled to a different-sized disc (disc d), whose resonance is detuned from the others by an energy ω_d , as in Ref. [52], but with two reservoirs instead of one. We calculate the transmission from one chain to the other, $\mathcal{T}(\omega)$, to find the perfectly-transmitting states.

We define $\omega = E - E_0$, where E is the injected microwave's energy, and E_0 is the energy of the middle of the reservoir's band (given by the energy of the mode of a reservoir disc in isolation). Then if disc d couples to disc n in reservoir $\alpha \in \{L, R\}$, the reservoir's spectral function is proportional to the local density-of-states at disc n in the reservoir [53]. As shown in Fig. 2b, these are [52]

$$J_\alpha^{(n)}(\omega) = \begin{cases} \frac{K \sin^2(n\varphi_y)}{\sqrt{1-y^2}} & \text{for } |y| \leq 1, \\ 0 & \text{for } |y| \geq 1, \end{cases} \quad (8)$$

where $y = \omega/\omega_c$ and $\varphi_y = \arccos[y]$, which means [52]

$$\Lambda_\alpha^{(n)}(\omega) = \begin{cases} \frac{\pi K \sin[2n\varphi_y]}{2\sqrt{1-y^2}} & \text{for } |y| \leq 1, \\ \pi K \frac{1 - (y\mathcal{A}(y) - y)^{2n}}{2y\mathcal{A}(y)} & \text{for } |y| \geq 1, \end{cases} \quad (9)$$

where $\mathcal{A}(y) = \sqrt{1-y^2}$. For $n \rightarrow \infty$, one has $J_\alpha^{(n \rightarrow \infty)}(\omega) = \text{Re}[K/2\sqrt{1-y^2}]$. Hence, $\Lambda_\alpha^{(n \rightarrow \infty)}(\omega) = \text{Re}[\pi K/(2y\mathcal{A}(y))]$, which is zero inside the band.

The transmission function, $\mathcal{T}(\omega)$, is then given by Eq. (4). For all $n < \infty$, if the energy of disk d is outside the band ($|\omega_d| > \omega_c$), then the transmission at all ω is very small at weak-coupling, see the grey curves in Fig. 3. It is surprising to find that once the coupling exceeds a critical value, then $\mathcal{T}(\omega) = 1$ at certain values of ω inside the band (marked by inverted black triangles in Fig. 3). This means that microwaves injected into reservoir L at these energies will be perfectly transmitted into reservoir R (without any reflection), despite passing through disk d whose energy is not even within the band.

Fig. 4 shows the phase diagram of perfectly-transmitting states for various n . At strong coupling, there are $(2n-1)$ such states (in addition to two bound-states outside the band) whether disc d 's energy is in the band or not, because Eq. (9) has $(2n-1)$ zeros in the band.

As the coupling grows, every alternate perfectly transmitting state broadens to a width of the order of the distance between peaks, however the other peaks move towards energies where $J_\alpha(\omega)$ vanishes, and so become extremely sharp. If one fine-tunes the dot energy ω_d one can align one of these states exactly at an energy where $J_\alpha(\omega)$ vanishes, at which point it becomes a ‘‘bound state in the continuum’’ [54] of the type discussed in Ref. [52]. However, the perfectly-transmitting states are always present and do not require any such fine-tuning.

For $n \rightarrow \infty$, the peaks become so densely packed that the transmission becomes smooth, and $J_\alpha^{(n \rightarrow \infty)}(\omega)$ has a square-root divergence at $\omega = \pm\omega_c$. Then there are perfectly transmitting states at the band-edges [9] at all K .

Graphene reservoirs. – Electronic systems rarely exhibit a single band well-separated from all others. Here we show we do not require this, the same physics can be seen when the reservoirs simply have a strong peak in their

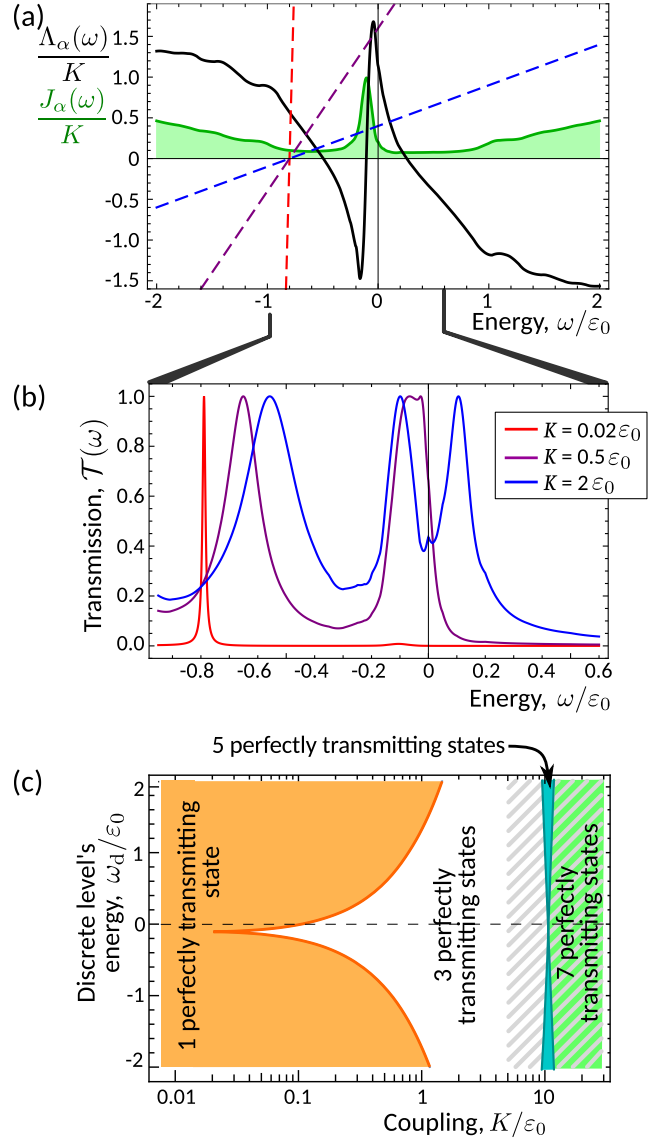


Fig. 5: (a) The spectral function $J_\alpha(\omega)/K$ (green curve) taken from Fig. 2c of Ref. [55], and $\Lambda_\alpha(\omega)/K$ (black curve) that we calculate from it. The dashed lines are $(\omega - \omega_d)/K$ for $\omega_d/\epsilon_0 = -0.8$ and $K/\epsilon_0 = 0.02, 0.5, 2$. Perfectly-transmitting states, given by Eq. (7), occur when the dashed lines intersect the black curve. (b) Plot of the transmission $\mathcal{T}(\omega)$ for $\omega_d/\epsilon_0 = -0.8$. For small K , it is a single Lorentzian peak at $\omega = \omega_d$, which broadens and moves as K increases. A transition occurs (at $K/\epsilon_0 = 0.45$) at which two more perfectly-transmitting states appear. (c) Phase diagram showing the number of such states as a function of ω_d and K .

spectral function, $J_\alpha(\omega)$. For this, we consider a single-level quantum dot between the zigzag edges of graphene reservoirs, under strong magnetic field. We take an experimental plot of $J_\alpha(\omega)$ from Ref. [55], reproduced as the green curve in Fig. 5a, which exhibits a strong peak. This curve comes from a STM measurement of the tunneling density-of-states of graphene's zigzag edge in the quantum Hall regime (4 Tesla at 4.4 Kelvin) [55]. A similar

peak was seen at the zigzag edge of a hexagonal lattice of microwave cavities [50]. This peak is specific to the edge; the bulk's density of states is very different, and vanishes at the Dirac point ($\omega = 0$ in Fig. 5). At sub-Kelvin temperatures, the dot's spin-splitting at 4 Tesla will be much bigger than temperature, so we can take a single-level dot whose upper spin-state is empty at all times, making the dot well modelled by Eq. (1). The STM measurement gives us $J_\alpha(\omega)$ for $|\omega| < 2\varepsilon_0$ where $\varepsilon_0 = \sqrt{2e\hbar v_F^2 B}$ [55]. We extrapolate this phenomenologically to $|\omega| > 2\varepsilon_0$ as $\alpha|\omega| \exp[-|\omega|/\omega_c]$ with $\omega_c = 10\varepsilon_0$ and α matching the gradient at $\omega = \pm 2\varepsilon_0$. Numerically integrating over this $J_\alpha(\omega)$, gives the $\Lambda_\alpha(\omega)$ in Fig. 5a, and the dot's transmission in Fig. 5b, to be observed experimentally with conductance measurements, see Eq. (6).

For small K , there is one perfectly-transmitting state on-resonance (at the energy of the dot, ω_d). However as K is increased, there is a transition to three such states. The phase diagram in Fig. 5c shows up to seven such states for large coupling K . However, the physics at large K depends on $J_\alpha(\omega)$ at large $|\omega|$, and so depends on our chosen extrapolation beyond the experimental data at $|\omega| > 2\varepsilon_0$. As such, the cross-hatched region of Fig. 5c may not agree with the experiments.

Comparison with local density-of-states. –

When $J_R(\omega) = J_L(\omega)$, the local density-of-states of the discrete-level is $\mathcal{T}(\omega)/(2\pi^2 J_L(\omega))$. Hence we see that the peaks of the local density-of-states will not coincide with the perfectly-transmitting states, unless $1/J_L(\omega)$ has a very weak ω dependence at the ω in question. In particular, when $J_\alpha(\omega)$ has a square-root divergence (such as for $n \rightarrow \infty$ in Eq. (8) or at the edge of the superconducting gap), the local density-of-states of the discrete-level vanishes, even though there is a perfectly-transmitting state there. Conversely, the factor of $1/J_L(\omega)$ in the local density-of-states means that it could have a peak at a value of ω which does not satisfy Eq. (7), if $J_L(\omega)$'s gradient is large at this ω . Ref. [38] used Eq. (7) as a heuristic method of finding peaks in the local density-of-states. The examples here show that this method is imprecise for such peaks (particularly at large K), when it is exact for perfectly-transmitting states at all K .

Hand-waving picture. – To see why there are multiple perfectly-transmitting states, imagine replacing a peak in $J_\alpha(\omega)$ of height K and width Ω with a Dirac δ -function on a flat background, so $J_\alpha(\omega) \rightarrow K\Omega\delta(\omega-\omega_1)+K_0$. Then $\Lambda(\omega) = 2K\Omega/(\omega-\omega_1)$, giving three perfectly transmitting states at energies ω_1 and $\omega_\pm = \omega_1 + \frac{1}{2}[\omega_d \pm \sqrt{\omega_d^2 + 8K\Omega}]$. This can be explained by treating the δ -peaks as a single level in each reservoir. These fictitious levels at energy ω_1 each have tunnel coupling $\sqrt{K\Omega}$ to the discrete-level at ω_d . Solving this three-level system will give three eigenstates with energies; ω_1 and ω_\pm . If K_0 is small enough that those three eigenstates have a golden-rule coupling to the remaining reservoir modes, it explains three perfectly-

transmitting states at these energies.

Replacing finite-width peaks in $J_\alpha(\omega)$ with δ -peaks gets some features right for coupling much greater than the peak width, $K \gg \Omega$. It correctly gives the solutions of Eq. (7) at $\omega \gg \omega_c$ for $K/\omega_c \rightarrow \infty$. It also correctly predicts that one solution will be at the centre of the spectral function's peak (i.e. at $\omega = \omega_1$) for $K \gg \omega_c, \omega_d$.

This approximation can be improved by taking Lorentzians in place of δ functions. Indeed, this is a reasonable approximation for the peak in the experimental $J_\alpha(\omega)$ in Fig. 5. Then $J_\alpha(\omega) = K_\alpha\Omega^2/((\omega-\omega_1)^2 + \Omega^2)$, so Eq. (5) gives the Lamb shift [2, 44]

$$\Lambda_\alpha(\omega) = \frac{\pi K_\alpha\Omega (\omega - \omega_1)}{(\omega - \omega_1)^2 + \Omega^2}. \quad (10)$$

Its qualitative features are a negative dip at $(\omega - \omega_1) \sim -\Omega$, growth through zero at $\omega \sim \omega_1$ and a positive peak at $(\omega - \omega_1) \sim \Omega$. These qualitative features are the same for other-shaped peaks in $J_\alpha(\omega)$, such as in Fig. 2b.

A more sophisticated approach in the same spirit is the “reaction coordinate mapping” [56, 57], recently used [44] on models like our Eq. (1). Unfortunately, this mapping did not simplify the calculations presented in this work.

Conclusions. – We show that a discrete-level strongly coupled to two reservoirs can exhibit multiple perfectly-transmitting states, as if it were a multi-level system. Even when the discrete-level is at an energy outside the reservoirs' bands, such states can appear when the coupling exceed a critical value, allowing perfect (reflectionless) flow between the two reservoirs. We propose observing this in electronic and microwave systems.

This model is a good testing ground for quantum thermodynamics at strong coupling [6, 8, 58–61], since the non-Markovian dynamics has such clear physical consequences for both bound states and perfectly-transmitting states. Some of the consequences for thermoelectric effects have been studied [9], but they merit further consideration.

Acknowledgements. – We thank A.N. Jordan, H. Kurkjian, A. Nazir and G. Shaller for useful discussions. We acknowledge the support of the French research program ANR-15-IDEX-02, via the Université Grenoble Alpes' QuEnG project.

REFERENCES

- [1] APERTET Y., OUERDANE H., GOUPIL C. and LECOEUR P., *Phys. Rev. E*, **85** (2012) 031116.
- [2] TOPP G. E., BRANDES T. and SCHALLER G., *EPL*, **110** (2015) 67003.
- [3] KATZ G. and KOSLOFF R., *Entropy*, **18** (2016) 186.
- [4] STRASBERG P. and ESPOSITO M., *Phys. Rev. E*, **95** (2017) 062101.
- [5] STRASBERG P., SCHALLER G., SCHMIDT T. L. and ESPOSITO M., *Phys. Rev. B*, **97** (2018) 205405.
- [6] WHITNEY R. S., *Phys. Rev. B*, **98** (2018) 085415.

- [7] DOU W., OCHOA M. A., NITZAN A. and SUBOTNIK J. E., *Phys. Rev. B*, **98** (2018) 134306.
- [8] SEIFERT U., *Phys. Rev. Lett.*, **116** (2016) 020601.
- [9] JUSSIAU É., HASEGAWA M. and WHITNEY R., *Phys. Rev. B*, **100** (2019) 115411.
- [10] BENENTI G., CASATI G., SAITO K. and WHITNEY R. S., *Phys. Rep.*, **694** (2017) 1.
- [11] STEFANUCCI G., *Phys. Rev. B*, **75** (2007) 195115.
- [12] ZHANG W.-M., LO P.-Y., XIONG H.-N., TU M. W.-Y. and NORI F., *Phys. Rev. Lett.*, **109** (2012) 170402.
- [13] JOHN S. and WANG J., *Phys. Rev. Lett.*, **64** (1990) 2418.
- [14] JOHN S. and WANG J., *Phys. Rev. B*, **43** (1991) 12772.
- [15] JOHN S. and QUANG T., *Phys. Rev. A*, **50** (1994) 1764.
- [16] KOFMAN A. G., KURIZKI G. and SHERMAN B., *J. Mod. Opt.*, **41** (1994) 353.
- [17] ANGELAKIS D. G., KNIGHT P. L. and PASPALAKIS E., *Contemp. Phys.*, **45** (2004) 303.
- [18] CHANG D. E., DOUGLAS J. S., GONZÁLEZ-TUDELA A., HUNG C.-L. and KIMBLE H. J., *Rev. Mod. Phys.*, **90** (2018) 031002.
- [19] XIONG H.-N., LO P.-Y., ZHANG W.-M., FENG D. H. and NORI F., *Sci. Rep.*, **5** (2015) 13353.
- [20] SHIBA H., *Prog. Theor. Phys.*, **50** (1973) 50.
- [21] MAHAN G. D., *Many-particle physics* 3rd Edition (Springer) 2000 Section 4.2 of either the 2nd edition (1990) or 3rd edition (2000).
- [22] LEI C. U. and ZHANG W.-M., *Ann. Phys.*, **327** (2012) 1408.
- [23] ALI M. M., LO P.-Y., TU M. W.-Y. and ZHANG W.-M., *Phys. Rev. A*, **92** (2015) 062306.
- [24] ALI M. M. and ZHANG W.-M., *Phys. Rev. A*, **95** (2017) 033830.
- [25] MACIEJKO J., WANG J. and GUO H., *Phys. Rev. B*, **74** (2006) 085324.
- [26] DHAR A. and SEN D., *Phys. Rev. B*, **73** (2006) 085119.
- [27] JIN J., TU M. W.-Y., ZHANG W.-M. and YAN Y., *New J. Phys.*, **12** (2010) 083013.
- [28] YANG P.-Y., LIN C.-Y. and ZHANG W.-M., *Phys. Rev. B*, **92** (2015) 165403.
- [29] TU M. W.-Y., AHARONY A., ENTIN-WOHLMAN O., SCHILLER A. and ZHANG W.-M., *Phys. Rev. B*, **93** (2016) 125437.
- [30] ENGELHARDT G., SCHALLER G. and BRANDES T., *Phys. Rev. A*, **94** (2016) 013608.
- [31] LIN Y.-C., YANG P.-Y. and ZHANG W.-M., *Sci. Rep.*, **6** (2016) 34804.
- [32] BASKO D. M., *Phys. Rev. Lett.*, **118** (2017) 016805.
- [33] LIU Y. and HOUCK A. A., *Nat. Phys.*, **13** (2017) 48.
- [34] KRINNER L., STEWART M., PAZMIÑO A., KWON J. and SCHNEBLE D., *Nature*, **559** (2018) 589.
- [35] COHEN-TANNOUDJI C., DUPONT-ROC J. and GRYNBERG G., *Atom-photon interactions: Basic process and applications* (Wiley) 1998 See sections I.B.2 and IV.C.
- [36] FANO U., *Phys. Rev.*, **124** (1961) 1866.
- [37] ANDERSON P. W., *Phys. Rev.*, **124** (1961) 41.
- [38] COHEN-TANNOUDJI C., DUPONT-ROC J. and GRYNBERG G., *Atom-photon interactions: Basic process and applications* (Wiley) 1998 See complement C_{III} at the end of chapter III (pp. 239-255).
- [39] MEIR Y. and WINGREEN N. S., *Phys. Rev. Lett.*, **68** (1992) 2512.
- [40] RYNDYK D. A., GUTIÉRREZ R., SONG B. and CUNIBERTI G., *Green function techniques in the treatment of quantum transport at the molecular scale in Energy Transfer Dynamics in Biomaterial Systems, Springer Series in Chemical Physics 93*, edited by BURGHARDT I., MAY V., MICHA D. and BITTNER E., (Springer-Verlag, Berlin) 2009 pp. 213–335 Particularly Section 2 of this chapter, whose Eprint is arXiv:0805.0628.
- [41] LANDAUER R., *IBM J. Res. Dev.*, **1** (1957) 223.
- [42] LANDAUER R., *Philos. Mag.*, **21** (1970) 863.
- [43] CAROLI C., COMBESCOT R., NOZIÈRES P. and SAINT-JAMES D., *J. Phys. C*, **4** (1971) 916.
- [44] MARTENSEN N. and SCHALLER G., *Eur. Phys. J. B*, **92** (2019) 30.
- [45] WILLIAMS J. R., DICARLO L. and MARCUS C. M., *Science*, **317** (2007) 638.
- [46] CHEN J., QIN H. J., YANG F., LIU J., GUAN T., QU F. M., ZHANG G. H., SHI J. R., XIE X. C., YANG C. L., WU K. H., LI Y. Q. and LU L., *Physical Review Letters*, **105** (2010) 176602.
- [47] LEMME M. C., KOPPENS F. H. L., FALK A. L., RUDNER M. S., PARK H., LEVITOV L. S. and MARCUS C. M., *Nano Letters*, **11** (2011) 4134.
- [48] O’LEARY D. P. and STEWART G. W., *J. Comput. Phys.*, **90** (1990) 497.
- [49] LAURENT D., LEGRAND O., SEBBAH P., VANNESTE C. and MORTESSAGNE F., *Phys. Rev. Lett.*, **99** (2007) 253902.
- [50] KUHL U., BARKHOFEN S., TUDOROVSKIY T., STÖCKMANN H.-J., HOSSAIN T., DE FORGES DE PARNY L. and MORTESSAGNE F., *Phys. Rev. B*, **82** (2010) 094308.
- [51] BARKHOFEN S., BELLEC M., KUHL U. and MORTESSAGNE F., *Phys. Rev. B*, **87** (2013) 035101.
- [52] LONGHI S., *Eur. Phys. J. B*, **57** (2007) 45.
- [53] HOEKSTRA H. J. W. M., *Surf. Sci.*, **205** (1988) 523.
- [54] HSU C. W., ZHEN B., STONE A. D., JOANNOPOULOS J. D. and SOLJAČIĆ M., *Nat. Rev. Mater.*, **1** (2016) 1.
- [55] LI G., LUICAN-MAYER A., ABANIN D., LEVITOV L. and ANDREI E. Y., *Nat. Commun.*, **4** (2013) 1744.
- [56] ILES-SMITH J., LAMBERT N. and NAZIR A., *Phys. Rev. A*, **90** (2014) 032114.
- [57] NAZIR A. and SCHALLER G., *The Reaction Coordinate Mapping in Quantum Thermodynamics in Thermodynamics in the Quantum Regime. Fundamental Theories of Physics, Vol 195*, edited by BINDER F., CORREA L., GOGOLIN C., ANDERS J. and ADESSO G., (Springer, Cham) 2018 pp. 551–577 Eprint at arXiv:1805.0830.
- [58] LUDOVICO M. F., LIM J. S., MOSKALETS M., ARRACHEA L. and SÁNCHEZ D., *Phys. Rev. B*, **89** (2014) 161306.
- [59] ESPOSITO M., OCHOA M. A. and GALPERIN M., *Phys. Rev. Lett.*, **114** (2015) 080602.
- [60] BRUCH A., THOMAS M., VIOLA KUSMINSKIY S., VON OPPEN F. and NITZAN A., *Phys. Rev. B*, **93** (2016) 115318.
- [61] LUDOVICO M. F., MOSKALETS M., SÁNCHEZ D. and ARRACHEA L., *Phys. Rev. B*, **94** (2016) 035436.

SUPPLEMENTARY MATERIAL

Appendix A: Simpler form of Eqs. (8,9). – The spectral function, $J_\alpha^{(n)}(\omega)$, and the associated Lamb shift $\Lambda_\alpha^{(n)}(\omega)$ for the n th site in a one dimensional chain are given in compact forms by Eq. (8,9), where we recall that $y \equiv \omega/\omega_c$. However, these are not the most transparent forms for energies inside the band, $|y| \leq 1$. There one can use the fact $\cos \varphi_y = y$ with the multiple angle formulas in trigonometry to write the expressions in terms of polynomials in y . Then the spectral functions inside the band ($|y| \leq 1$) for small integer n are

$$J_\alpha^{(n=1)}(\omega) = K_\alpha \sqrt{1-y^2}, \quad (11)$$

$$J_\alpha^{(n=2)}(\omega) = K_\alpha \sqrt{1-y^2} 4y^2, \quad (12)$$

$$J_\alpha^{(n=3)}(\omega) = K_\alpha \sqrt{1-y^2} (1-4y^2)^2, \quad (13)$$

$$J_\alpha^{(n=4)}(\omega) = K_\alpha \sqrt{1-y^2} 16y^2(1-2y^2)^2, \quad (14)$$

with $y \equiv \omega/\omega_c$. We see that the second factor is an $(n-1)$ -degree polynomial of y^2 ; so it becomes increasingly unpleasant to handle as n grows. Similarly, the Lamb shifts inside the band ($|y| \leq 1$) for these integer n are

$$\Lambda_\alpha^{(n=1)}(\omega) = \pi K_\alpha y, \quad (15)$$

$$\Lambda_\alpha^{(n=2)}(\omega) = -2\pi K_\alpha y(1-2y^2), \quad (16)$$

$$\Lambda_\alpha^{(n=3)}(\omega) = \pi K_\alpha y(3-16y^2+16y^4), \quad (17)$$

$$\Lambda_\alpha^{(n=4)}(\omega) = -4\pi K_\alpha y(1-2y^2)(1-8y^2+8y^4). \quad (18)$$

We see that this is y times an $(n-1)$ -degree polynomial of y^2 , so it is always odd in y . These polynomials have $(2n-1)$ zeros in the window $|y| \leq 1$, as is most easily seen by counting the zeros of $\sin[2n\varphi_y]$ in Eq. (9).

Appendix B: Other simple examples of $\Lambda(\omega)$. – Phenomenologically, the simplest model of a single band is to assume its spectral function takes the form

$$J_\alpha(\omega) = \begin{cases} K (1 - (\omega/\omega_c)^2)^s & \text{for } |\omega| \leq \omega_c, \\ 0 & \text{for } |\omega| > \omega_c, \end{cases} \quad (19)$$

where s determines how the spectral function behaves at the band edges. For certain values of s , one can directly evaluate the integral in Eq. (5). Examples are

$$\Lambda_\alpha(\omega) = \begin{cases} K \left(\frac{\omega_c^2 - \omega^2}{\omega_c^2} \ln \left| \frac{\omega_c + \omega}{\omega_c - \omega} \right| + \frac{2\omega}{\omega_c} \right) & \text{for } s = 1 \\ \frac{\pi K \omega}{\omega_c} \left(1 - \text{Re} \left[\sqrt{1 - (\omega_c/\omega)^2} \right] \right) & \text{for } s = \frac{1}{2} \\ K \ln \left| \frac{\omega_c + \omega}{\omega_c - \omega} \right| & \text{for } s = 0 \\ \frac{\pi K \omega_c}{\omega} \text{Re} \left[\left(1 - (\omega_c/\omega)^2 \right)^{-1/2} \right] & \text{for } s = -\frac{1}{2} \end{cases} \quad (20)$$

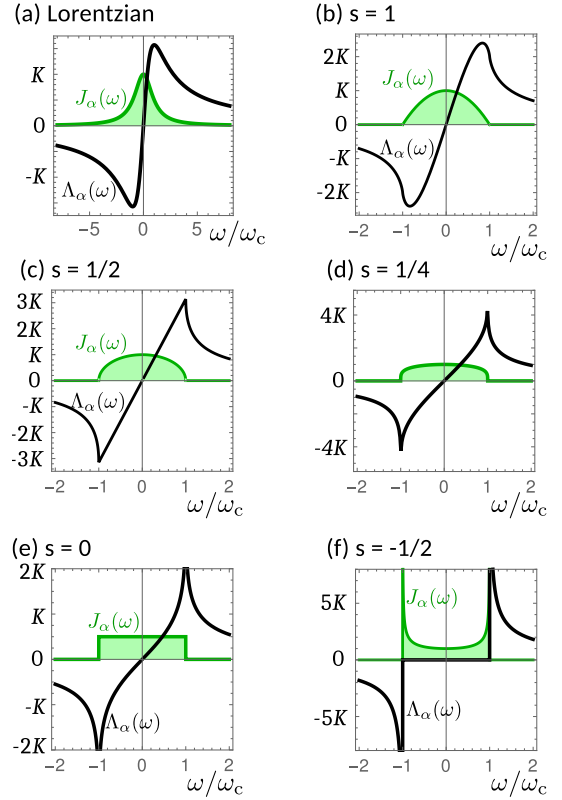


Fig. 6: Plots of various spectral functions, $J_\alpha(\omega)$ (green curve) and the associated Lamb shift, $\Lambda_\alpha(\omega)$ (black curve). In (a) we plot a Lorentzian $J_\alpha(\omega)$, with the $\Lambda_\alpha(\omega)$ in Eq. (10). In (b) to (f) we plot $J_\alpha(\omega)$ in Eq. (19) for different values of the spectral exponent, s , with the $\Lambda_\alpha(\omega)$ for most given in Eq. (20).

where the positive square-root is taken, and the real parts are zero for $|\omega| < \omega_c$. These are shown in Fig. 6. The results for $s = \pm 1/2$ were given elsewhere [19,21,28], however it is intriguing that the Lamb shift inside the band is strictly zero for $s = -1/2$.

Appendix C: When the strongest coupling does not have the most perfectly-transmitting states.

– The spectral functions treated in the body of this work have the maximum number of perfectly-transmitting states when the discrete-level's coupling to the reservoir is strongest. This is not always the case. Here we mention situations with more perfectly-transmitting states at weak or intermediate coupling than at strong coupling.

For spectral function, $J_\alpha(\omega)$, given by Eq. (19) with $-1/2 < s \leq 0$, one can see that $\Lambda(\omega)$ diverges at the band-edge, and its gradient inside the band is not a concave function of ω . Hence within the band, there can be multiple intersections between $\Lambda(\omega)$ and the straight line $(\omega - \omega_d)$, even at weak-coupling (small or vanishing K); implying multiple solutions of Eq. (7) inside the band (i.e. perfectly-transmitting states) when the coupling goes to zero, $K \rightarrow 0$. This can be seen for $s = 0$ in Fig. 6e, where a straight line will always intersect $\Lambda(\omega)$ twice outside the band (i.e. two bound states), and will

intersect $\Lambda(\omega)$ up to three times inside the band (i.e. up to three perfectly-transmitting states). There are always three perfectly-transmitting states at weak-coupling, but only one perfectly-transmitting state above a certain critical coupling. The transition from three to one perfectly-transmitting states occurs when two such states converge and annihilate (a transition of type ii).

The fact that there are five solutions of Eq. (7) (two bound-states and three perfectly-transmitting states) at arbitrarily small coupling is a drastic indication that the golden-rule (which never predicts more than one such solution) fails even at vanishing coupling. A similar failure was already noted when there is a square-root divergence at the band-edge [9], because $J(\omega)$ exhibits a divergence. Now we can see that such a failure of golden-rule can also occur when $\Lambda(\omega)$ exhibit a divergence (even if $J(\omega)$ is convergent).

If there is no divergence in $J(\omega)$ or $\Lambda(\omega)$, then the golden rule will work at small coupling, and there will only be a single solution of Eq. (7) in the weak-coupling limit, $K \rightarrow 0$. This solution's energy will be extremely close to ω_d , so it will correspond to a bound-state if ω_d is outside the band, and a perfectly-transmitting state if ω_d is inside the band. However, in this case, it is not difficult to find examples in which the maximum number of perfectly-transmitting states occurs at intermediate coupling. Imagine taking almost any case where $\Lambda(\omega)$ does not diverge and is not a straight line inside the band, such as $s = 1$ or $s = 1/4$ in Fig. 6, or indeed taking any $-1/2 < s \leq 0$ with added rounding at the band-edge so divergences in $J(\omega)$ or $\Lambda(\omega)$ are replaced by large peaks. Then it is easy to find situations with ω_d close to the band centre in which there is;

- one perfectly-transmitting state with no bound states at small coupling,
- three perfectly-transmitting states and two bound states at intermediate coupling,
- one perfectly-transmitting state and two bound states at large coupling.

So there are more such states at intermediate level-reservoir coupling than at large or small coupling.